Article:

ORIGINAL RESEARCH

Modelling, control design, and analysis of the inner control's loops intended for single-phase voltage-controlled inverter-based microgrid

Camelia Ait Hammouda[1] | Rafik Bradai[1] | Ahmed Bendib[2] | Abdelhammid Kherbachi[3] | Kamel Kara[2] | Rachid Boukenoui[2] | Hafiz Ahmed[4]

[1]LATSI Laboratory, Renewable Energies Department, Blida1 University, Blida, Algeria

[2]SET Laboratory, Electronics Department, Blida1 University, Blida, Algeria

[3]Renewable Energy Development Center, Algiers, Algeria

[4]The University of Sheffield, Nuclear AMRC Midlands, Derby, UK

Correspondence

Hafiz Ahmed, University of Sheffield, Nuclear AMRC Midlands, Rutherford Way, Infinity Pk Wy, Derby DE73 5SS, UK.
Email: hafiz.ahmed@sheffield.ac.uk;
hafiz.h.ahmed@ieee.org

Abstract

In voltage-controlled voltage source inverters (VSIs)-based microgrids (MGs), the inner control is of prime interest task for guaranteeing safe and stable operation. In this paper, an in-depth investigation of the modelling, control design, and analysis of the voltage and current inner control loops intended for single-phase voltage-controlled VSIs is established. The main objective of this work is to provide a comprehensive study of the mathematical modelling, control design, and performance evaluation of the inner control's loops considering different proportional-integral (PI) controller types with and without compensation, and to determine the optimal scheme that can offer better performance in terms of implementation simplicity, robustness, and transient and steady-state responses. Thus, the mathematical closed-loop models of designed outer voltage and inner current control schemes based on PI, P, and feedforward controllers with and without compensation are, first, derived. Following this, a systematic and effective control design for tuning the different PI controllers' parameters is proposed. Furthermore, an analysis revealing the performance of the designed voltage and current control schemes is provided. This analysis enables us to choose a P controller and PI feedforward controller for the current control loop and the voltage control loop, respectively. The chosen P and PI controllers should be simple; meanwhile, they should offer a wide bandwidth. A simulation study is carried out in MATLAB/Simulink software to assess the performance of the adopted inner control scheme for both linear and non-linear loads. In addition, an experimental setup, based on a TMS320F2837xD μC, of a single-phase VSI supplying linear and non-linear loads is built to verify the effectiveness and the robustness of the adopted inner controller. The results demonstrated: (1) the necessity of introducing the compensation term, which is responsible for offering control improvement against voltage perturbation, (2) the high tracking performance of the chosen controller in terms of dynamic and steady-state responses as well as its simplicity of implementation.

1 | INTRODUCTION

High-energy losses in power generation and transmission, high generation costs, carbon emissions, environmental concerns, and high investment costs for grid expansion are all serious issues in conventional power systems [1]. However, deep inte-

gration of renewable energy sources (RES) in the energy sector can help to reduce greenhouse gas emissions by at least 55% compared to 1990 [2]. In this regard, the concept of microgrids (MGs) has been introduced for promoting distributed energy resources (DERs). They work like a small-scale power grid that integrates a variety of renewable DERs as a plan to

meet new environmental criteria imposed by state authorities [3, 4]. Besides, the MGs have the possibility of working in two modes, connected to the grid or islanded [5–7]. Often, power electronic converters are employed as an interface for connecting DERs to the MG bus, the main grid network, and/or local loads. More particularly, voltage source inverters (VSIs) are the most common converters used for connecting distributed generators (DGs) to the MG via an LC filter, especially when energizing critical loads in islanded mode [8, 9]. Considering islanded mode, a local controller called primary control is generally adopted for VSIs' output voltage regulation as well as the control of power balance among DG units. This control level includes two main control units, the power-sharing control bloc based on the droop control strategy, intended for regulating the voltage magnitude and frequency based on the requested load power in parallel-connected DGs, and the inner controller which is detailed in this paper [5, 10]. This controller is responsible for adjusting the inverter output voltage to the desired voltage reference (i.e. provided by the droop control) with good tracking performance and a high stability of the MG system. However, for achieving such objectives under different DGs' disturbances, the modelling and control design of the inner control, which are challenging tasks, should be carefully investigated.

Various conventional and advanced control techniques have been adopted for the inner control implementation intended for voltage-controlled VSIs-based MG [11–21]. Among them are classical linear control systems with single or multiple proportional-integral (PI) feedback/feedforward loops [11–16], proportional-resonant (PR) control strategies [17–19], and advanced control strategies, such as model predictive control (MPC) [20], and sliding mode control (SM) [21], etc. However, the double-loop inner control scheme based on the PI controller, which consists of cascaded external voltage and internal current control loops (CCLs), is the most popular technique that has been applied to regulate the output voltage of the voltage-controlled VSIs. In this scheme, the voltage and current controllers are often designed by employing either a simple PI regulator or the PI feedforward regulator; then, the modelling and control design-based stability analysis are investigated to select the controllers' parameters. For instance, the authors in [22] investigated the modelling and control design-based stability analysis of a P regulator employed as an inner CCL, and an integral-resonant (IR) regulator proposed as the outer voltage controller. This suggested controllers-based inner control scheme is applied for single-phase voltage-controlled inverters in grid-connected MGs. In [23], brief modelling and design of a dual-loop controller based on a P controller for the CCL and four different resonant regulators for the capacitor voltage control are considered for an LC-filtered voltage-controlled VSI. Stability analysis as well as control design of dual-loop and single-loop voltage PI controllers intended for voltage-controlled VSI are established in [24]. Researchers in [25] covered the modelling and design of the CCL and VCL by integrating a P and a PI controller in each loop, respectively. Both loops

are studied in $\alpha\beta$ frame for a three-phase voltage-controlled inverter.

The majority of the existing studies, unfortunately, have either provided brief modelling and design of the VCL and CCL or considered only the adopted type of the PI controller. In addition, the number of research works applied for single-phase voltage-controlled VSI is limited. Furthermore, the authors often investigated control design-based stability analysis considering the PI parameters change, which is difficult in the case of multi-loop control with several parameters. To this end, this paper provides an in-depth investigation of the modelling, control design, and analysis of four designed inner control schemes based on a PI and feedforward controller types for the VCL and a P, PI, and feedforward controller types for the CCL intended for an LC-filtered single-phase voltage-controlled VSI. The contributions made in this paper are

- The closed-loop models of the CCL and VCL considering different PI controller types, with and without compensation, are derived;
- A systematic control design-based stability analysis is developed to tune the parameters of each controller type. Also, in this design, unlike the existing methods, the stability assessment is carried out considering the settling time variations, not the controller parameter variations;
- Root-locus analysis is performed to evaluate the performance of each controller, which allows the selection of the appropriate controller type;
- The robustness of the chosen control scheme is verified with and without compensation terms and under various conditions.

To assess the selected controller tracking performance, a system is built in the MATLAB/SimPowerSystem environment. The given results demonstrate the robustness of the proposed controller for output voltage tracking with good performance in both steady-state and transient conditions and under various abnormalities. Then, to validate the proposed controller, an experimental test based on a TMS320F2837xD μC is done.

The rest of this paper is organized as follows: Section 2 describes the primary control scheme of single-phase voltage-controlled VSI-based MG. In Section 3, the modelling, control design, and analysis of the VCL and CCL are provided with the aid of a suggested guideline and analysis based on the root locus. Results and discussions are presented in Section 4. Section 5 introduces experimental tests based on a TMS320F2837xD MCU. The main conclusions of this work are summarized in Section 6.

2 | MODELLING AND CONTROL OF VOLTAGE-CONTROLLED VSIS

In this section, the structure and modelling of the voltage-controlled VSI system within AC MG are presented, and the respective inner control scheme is described.
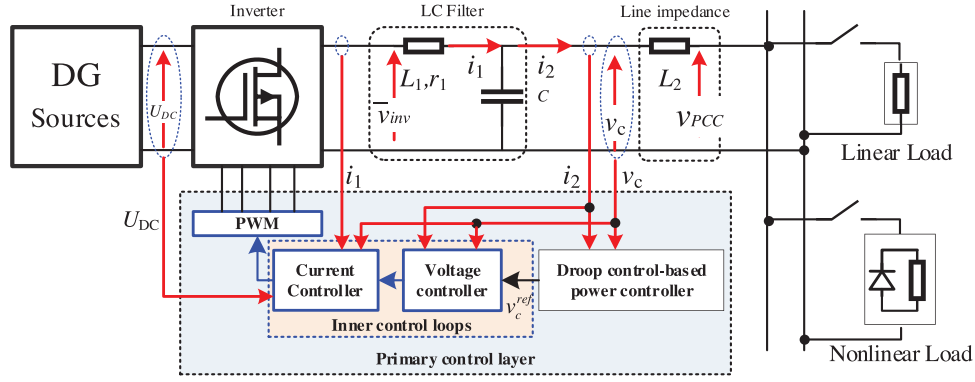
FIGURE 1 Schematic of the inner controller-based primary control for a single-phase VSI. VSI, voltage source inverters.

2.1 | Description of the system under study

The structure of the voltage-controlled single-phase VSI with the controller scheme including the double-loop inner controller is depicted in Figure 1. One can notice that the VSI with an LC filter stage is fed by a DC source, and linked to an AC bus or the point of common coupling (PCC), via a line impedance (L_2). In addition, this VSI supplies a load, which is tied to the MG AC bus. The control scheme consists of (1) a power controller based on the droop method and (2) an inner controller.

The droop control is in charge of providing the reference of the inverter output voltage according to the P/f and Q/V droop characteristics given below, with the help of a sinusoidal signal generator.

$$\omega = \omega^{ref} - mP_{mes} \tag{1}$$

$$E = E^{ref} - nQ_{mes} \tag{2}$$

where ω, E, ω^{ref}, and E^{ref} are the frequency and the magnitude of the inverter output voltage and their references, respectively, m and n are the droop gains, while P_{mes} and Q_{mes} are the measured active and reactive powers. More details about the droop controller can be found in [26].

The inner controller, which is the focus of this paper, is responsible for regulating the inverter output voltage to its reference, offered by the droop control block, and producing the expected voltage reference of the inverter to the PWM module that, in turn, generates the commands of the inverter's switches.

2.2 | LC-filtered VSI model

According to Figure 1, the mathematical model of the LC-filtered VSI can be derived as follows:

$$L_1 \frac{d}{dt} i_1(t) = \bar{v}_{inv}(t) - r_1 i_1(t) - v_c(t) \tag{3}$$

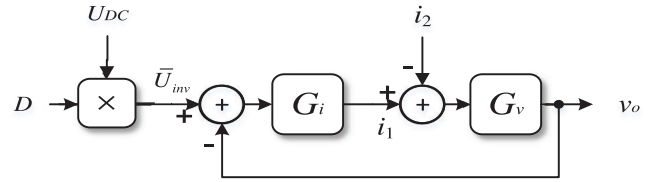$$C \frac{d}{dt} v_c(t) = i_1(t) - i_2(t) \tag{4}$$

FIGURE 2 Block diagram of the LC-filtered VSI average model. VSI, voltage source inverters.

$$\bar{v}_{inv}(t) = DU_{DC}(t) \tag{5}$$

where r_1, L_1, and C are the LC filter inductor resistance and inductance, and capacitor, i_1, and i_2 are the filter and output currents, $\bar{v}_{inv}$, v_c, and U_{DC} are the inverter average voltage, the output voltage, and the DC source voltage, and D is the duty cycle.

Considering these equations, the schematic diagram of the averaged model of the LC-filtered inverter in Laplace (s-domain) can be established as shown in Figure 2. The system model, as shown, includes the transfer functions of the filter inductor and capacitor, G_i and G_v which can be defined as follows:

$$\begin{cases} G_i = \frac{1}{r_1 + L_1 s} \\ G_v = \frac{1}{Cs} \end{cases} \tag{6}$$

where s denotes the Laplace operator, while the big symbols in Figure 2 define the average values of the respective variable.

2.3 | Inner control scheme

The inner control scheme, as shown in Figure 1, is a double-loop controller that consists of an external VCL and an internal CCL. The VCL is introduced for controlling the capacitor voltage and producing the current reference to the CCL. But, the CCL is intended for adjusting the inductor current to the reference generated by the first loop. These control loops are designed based on PI controllers; however, in order to ensure
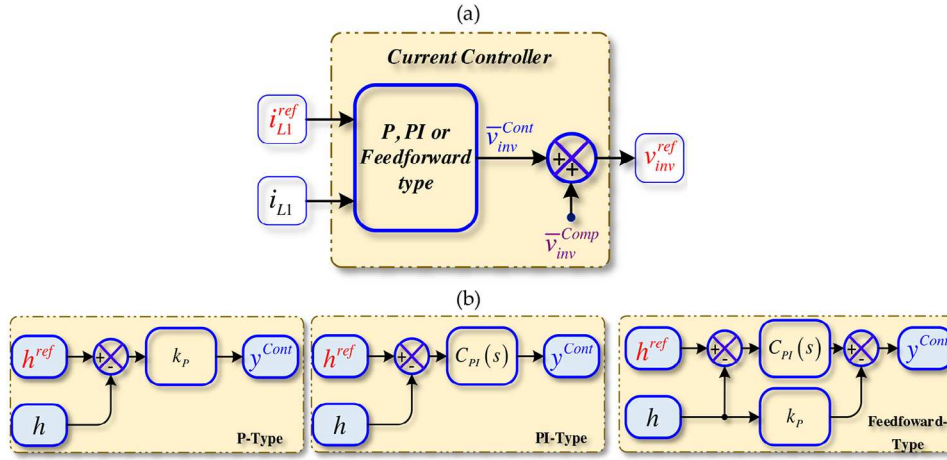
FIGURE 3 Block diagram of (a) the CCL, and (b) the P, PI, and feedforward controllers. CCL, current control loop.

simple implementation and good tracking performance, the type of the used PI controller should be carefully chosen and their parameters should be properly tuned. In addition, the compensation process is another essential issue that should be considered in the design of these control loops. To this end, the modelling and design of the VCL and CCL based on different PI controllers, with and without compensation, are investigated in the next section.

3 | MODELLING AND CONTROL DESIGN OF THE VCL AND CCL

The inner controller should ensure that the VSI module performs as a robust voltage source, in order to reduce the impact of VSIs' internal impedance on the system control performance. Therefore, in this section, the mathematical models of considered VCL and CCL are developed. These loops are based on three different controller types including P, PI, and PI feedforward controllers, as well as, with and without compensation terms. Further, a systematic and effective control design is provided for a proper tune of the controllers' parameters, in which the stability is analyzed considering the settling time variation instead of the controller parameters variation. Moreover, the robustness of the proposed controller against the variation of the system and controller parameters is elaborated. Finally, the discretization procedure of the adopted controller is given.

3.1 | Internal current control loop (CCL)

Figure 3a shows the schematic diagram of the CCL designed based on P, PI, or feedforward controllers with and without compensation, in which their structures are as depicted in Figure 3b. In this control loop, the actual current (i_{L1}) of the filter inductor and the corresponding current reference (i_{L1}^{ref}) are compared, and the resulting error is handled by one of the controllers; P, PI, or feedforward. In addition, the controller output is either considered directly as a reference without compensa-
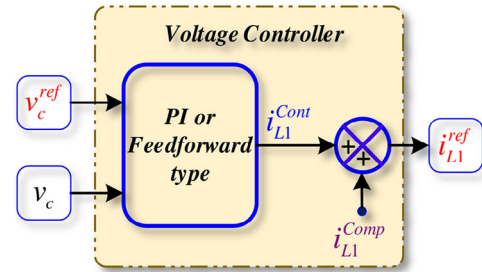

FIGURE 4 Block diagram of the VCL. VCL, voltage control loop.

tion or with the compensation term (v_c), to get the inverter side voltage reference.

According to Figure 3b, the expression of the current controller considering different types, P, PI, and PI feedforward, and the compensation term, can be obtained as follows:

P controller
$$\bar{v}_{inv}^{ref} = k_{p.i}\left(i_{L1}^{ref} - i_{L1}\right) + v_c \tag{7a}$$

PI controller
$$\bar{v}_{inv}^{ref} = C_i\left(s\right)\left(i_{L1}^{ref} - i_{L1}\right) + v_c \tag{7b}$$

PI feedforward controller
$$\bar{v}_{inv}^{ref} = C_i\left(s\right)\left(i_{L1}^{ref} - i_{L1}\right) - k_{p.i}i_{L1}^{ref} + v_c \tag{7c}$$

where $k_{p.i}$ and $k_{i,i}$ are the gains of the current controller, $\bar{v}_{inv}^{ref}$ is the voltage reference of the inverter side, and $C_i(s)$ is the transfer function of the PI controller which can be defined as follows:

$$C_i\left(s\right) = k_{p.i} + \frac{k_{i.i}}{s} \tag{8}$$

3.2 | Outer voltage control loop (VCL)

Figure 4 depicts the designed VCL scheme based on PI and PI feedforward controllers considering the compensation. As
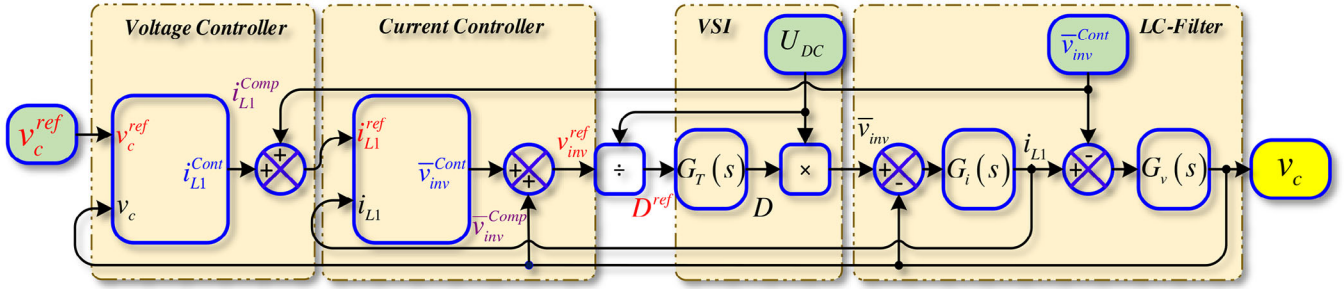
FIGURE 5 Closed-loop model of voltage-controlled LC-filtered VSI. VSI, voltage source inverters.

shown, the error is evaluated by comparing the actual output voltage (v_c) of the LC-filter capacitor and its reference (v_c^{ref}). This error is used by the controller to generate the output current reference, (i_{L1}^{ref}), in corporation with the current inductor (i_{L2}), which is the compensation term. Considering the PI and PI feedforward controllers and the compensation term, the expression of the voltage controller can be obtained as follows:

PI controller
$$i_{L1}^{ref} = C_v\left(v_c^{ref} - v_c\right) + i_{L2} \tag{9a}$$

PI feedforward controller
$$i_{L1}^{ref} = C_v\left(v_c^{ref} - v_c\right) - k_{p,v}v_c^{ref} + i_{L2} \tag{9b}$$

where $C_v(s)$ is the transfer function of a PI controller, which can be written as follows:

$$C_v(s) = k_{p,v} + \frac{k_{i,v}}{s} \tag{10}$$

where $k_{p,v}$ and $k_{i,v}$ are the voltage controller's gains.

3.3 | Closed-loop model

The schematic diagram of the closed-loop model of the voltage-controlled LC-filtered VSI including the inner control loops is illustrated in Figure 5. From this figure, the closed-loop model consists of the system model, that is, VSI with LC filter, the functions of the controllers, and the transfer function, $G_T(s)$, describing the time delay dynamics, which can be defined by its one of the simplest linear approximations given below:

$$G_T(s) = \frac{D(s)}{D^{ref}(s)} = \frac{1}{1+1.5T_s s} \tag{11}$$

where T_s denotes the sampling time, and D^{ref} is the duty ratio of the PWM, which can be defined as a function of the output voltage reference and the DC side voltage as follows:

$$D^{ref} = \frac{\bar{v}_{inv}^{ref}}{U_{DC}} \tag{12}$$

Based on Figure 4, the mathematical closed-loop models of the current and voltage controls can be expressed as follows:

TABLE 1 Expressions of G_i^{BF}, G_v^{BF}, H_i, $Z_{i,L1}$, and $Z_{i,L2}$.

		P-type	PI-type	Feedforward-type
Current control loop	G_i^{BF}	$\frac{k_{p,i}G_T G_i}{1+k_{p,i}G_T G_i}$	$\frac{C_i G_T G_i}{1+C_i G_T G_i}$	$\frac{(C_i-k_{p,i})G_T G_i}{1+C_i G_T G_i}$
	H_i	$\frac{G_i(G_T-1)}{1+k_{p,i}G_T G_i}$	$\frac{G_i(G_T-1)}{1+C_i G_T G_i}$	$\frac{G_i(G_T-1)}{1+C_i G_T G_i}$
Voltage control loop	G_v^{BF}	$\frac{k_{p,v}G_i^{BF}G_v}{1+k_{p,v}G_i^{BF}G_v}$	$\frac{C_v G_i^{BF}G_v}{1+C_v G_i^{BF}G_v}$	$\frac{(C_v-k_{p,v})G_i^{BF}G_v}{1+C_v G_i^{BF}G_v}$
	$Z_{i,L1}$	$\frac{G_p H_i}{1+k_{p,v}G_i^{BF}G_v}$	$\frac{G_p H_i}{1+C_v G_i^{BF}G_v}$	$\frac{G_p H_i}{1+C_v G_i^{BF}G_v}$
	$Z_{i,L2}$	$\frac{k_{p,v}G_i^{BF}G_v}{1+k_{p,v}G_i^{BF}G_v}$	$\frac{C_v G_i^{BF}G_v}{1+C_v G_i^{BF}G_v}$	$\frac{C_v G_i^{BF}G_v}{1+C_v G_i^{BF}G_v}$

$$i_{L1} = G_i^{BF} i_{L1}^{ref} + H_i v_c \tag{13}$$

$$v_c = G_v^{BF} v_c^{ref} + Z_{i,L1}i_{L1} + Z_{i,L2}i_{L2} \tag{14}$$

where the transfer functions G_i^{BF}, G_v^{BF}, $H_i, Z_{i,L1}$, and $Z_{i,L2}$ can be defined, for each controller's type, as given in Table 1.

By substituting the expressions of these functions into (13) and (14), the voltage and current closed-loop models can be easily derived for each controller's type. By the way, these transfer functions are very useful for system stability analysis and control parameters tuning.

3.4 | Control design and parameters' tuning

Tuning a controller is an important task in the control system because good controller tuning can ensure high efficiency, low energy cost, increased production rate, and reduced process variability. This subsection proposes a systematic and effective control design for the tune of the controllers' parameters for steering the closed-loop response to satisfy preset time-domain desired specifications. Unlike the existing techniques, which perform parameters tuning-based stability analysis with random variation of the controller parameters (i.e. k_p, and k_i), the suggested method provides a systematic guideline for the parameters tuning with stability analysis considering the variation of the transient response settling time.

The first step in the guideline is to derive the simplified closed-loop model of both voltage and current controls.

TABLE 2 Simplified closed-loop transfer function of the current control.

	$G^{BF}_{i_{simplify}}$	$H_{i_{simplify}}$
P-type	$\dfrac{\frac{k_{p,i}}{L_1}}{s+\frac{k_{p,i}+r_1}{L_1}}$	0
PI-type	$\dfrac{\frac{k_{p,i}}{L_1}s+\frac{k_{i,i}}{L_1}}{s^2+\left(\frac{r_1+k_{p,i}}{L_1}\right)s+\frac{k_{i,i}}{L_1}}$	0
Feedforward-type	$\dfrac{\frac{k_{p,i}}{L_1}}{s^2+\left(\frac{r_1+k_{p,i}}{L_1}\right)s+\frac{k_{p,i}}{L_1}}$	0

TABLE 3 Simplified closed-loop transfer function of the voltage control.

	$G^{BF}_{v_{simplify}}$	$Z_{i.L1_{simplify}}$	$Z_{i.L2_{simplify}}$
PI-type	$\dfrac{\frac{k_{p,v}}{C}s+\frac{k_{I,v}}{C}}{s^2+\frac{k_{p,v}}{C}s+\frac{k_{I,v}}{C}}$	0	0
Feedforward-type	$\dfrac{\frac{k_{p,v}}{C}}{s^2+\frac{k_{p,v}}{C}s+\frac{k_{I,v}}{C}}$	0	0

By assuming that the time delay is very small compared to the current controller response time, and the CCL is considered in steady state, the transfer function of (11) results in

$$G_T(s)|_{Steady-state} = 1 \tag{15}$$

Hence, the closed-loop transfer functions of the current control given in Table 1, taking into consideration (6) and (8), can be simplified as presented in Table 2.

On the other hand, based on the hypothesis that the CCL is faster compared to the VCL, the CCL is considered in steady state and its closed-loop transfer function becomes

$$G^{BF}_{i_{simplify}}(s)\bigg|_{Steady-state} = 1 \tag{16}$$

Therefore, and by considering the transfer functions of the voltage control given in Table 1, the simplified closed-loop transfer function of the voltage control for each controller's type can be derived as given in Table 3.

From Table 2, the transfer function G^{BF}_i of each controller's type represents the simplified closed-loop mathematical model of the current control, in which, in the case of the P-type controller, it exhibits a first-order transfer function. While, in the case of the PI-type and feedforward-type controllers, it exhibits a second-order transfer function. Otherwise, according to Table 3, the transfer function G^{BF}_v of each controller's type defines the simplified closed-loop model of the voltage control, where it exhibits a second-order transfer function for both PI and feedforward controller types.

The second step, in the guideline, is determining the mathematical expressions of the controllers' parameters as a function of the settling time. By matching the derived closed-loop models, given in Tables 2 and 3, with desired first-order and second-order transfer functions, described by the following equations:

$$G^{BF}_{i_{desired}}(s) = k_i \frac{1}{\tau s + 1} \tag{17a}$$

$$G^{BF}_{i_{desired}}(s) = \frac{\omega_i^2}{s^2 + 2\zeta_i\omega_i s + \omega_i^2} \tag{17b}$$

$$G^{BF}_{v_{desired}}(s) = \frac{\omega_v^2}{s^2 + 2\zeta_v\omega_v s + \omega_v^2} \tag{17c}$$

The expressions of the parameters $k_i, \tau, \zeta_i, \omega_i, \zeta_v$, and ω_v can be defined as follows:

a. For the CCL

P-type Controller

$$\begin{cases} k_i = \dfrac{k_{p,i}}{k_{p,i}+r_1} \cong 1 \\ \tau = \dfrac{L_1}{k_{p,i}+r_1} \end{cases} \tag{18a}$$

PI and feedforward controllers

$$\begin{cases} \zeta_i = \dfrac{r_1+k_{p,i}}{2L_1\omega_i} \\ \omega_i = \sqrt{\dfrac{k_{i,i}}{L_1}} \end{cases} \tag{18b}$$

b. For the PI and feedforward type controllers of the VCL

$$\begin{cases} \zeta_v = \dfrac{k_{p,v}}{2C\omega_v} \\ \omega_v = \sqrt{\dfrac{k_{p,v}}{C_f}} \end{cases} \tag{19}$$

where $k_i, \tau, \zeta_i,$ and ω_i stand for the gain factor, the time constant, the damping factor, and the natural frequency of the inner current control, respectively. Also ζ_v and ω_v denote the damping factor and the natural frequency of the outer VCL.

Based on (18) and (19), the parameters of the CCL and VCL for each controller's type can be expressed as follows:

a. CCL
P-type controller

$$k_{p,i} \simeq \frac{L_1}{\tau} \tag{20a}$$

PI and feedforward controllers

$$\begin{cases} k_{p,i} = 2L_1\zeta_i\omega_i - r_1 \\ k_{i,i} = L_1\omega_i^2 \end{cases} \tag{20b}$$

b. PI-type and feedforward controllers of the VCL

$$\begin{cases} k_{p,v} = 2C\zeta_v\omega_v \\ k_{i,v} = C\omega_v^2 \end{cases} \tag{21}$$

On the other hand, the parameters $\tau, \zeta_i, \zeta_v, \omega_i,$ and ω_v can be described as a function of the transient response overshoot M_p and the settling time t_s as follows:

a. The CCL

$$\text{P-type Controller}$$
$$t_{s.i} = 4\tau \tag{22a}$$

$$\text{PI and feedforward controllers}$$
$$\begin{cases} M_{p.i} = e^{\frac{\zeta_i \pi}{\sqrt{1-\zeta_i^2}}} \\ t_{s.i} = \frac{4}{\zeta_i \omega_i} \end{cases} \tag{22b}$$

b. The PI-type and feedforward controllers of the VCL

$$\begin{cases} M_{p.v} = e^{\frac{\zeta_v \pi}{\sqrt{1-\zeta_v^2}}} \\ t_{s.v} = \frac{4}{\zeta_v \omega_v} \end{cases} \tag{23}$$

It is worth mentioning that the values of the damping factor and the settling time are chosen according to the analysis based on root-locus plots while considering the following conditions:

$$\begin{cases} f_n \langle\langle \frac{1}{t_{s.v}} \langle\langle \frac{1}{4t_{s.i}} \langle\langle f_{rs} \langle\langle \frac{f_{switch}}{2} \\ 0.4 \le \zeta_{i,v} \le 1 \end{cases} \tag{24}$$

where f_n, f_{rs}, and f_{switch} are the fundamental frequency, the LC-filter resonant frequency, and the inverter switching frequency. Also, $t_{s.i,v}$ and $\zeta_{i,v}$ are the current and voltage settling times and the damping factors, respectively.

By adjusting one of the parameters each time, the impact of each parameter on system performance is analyzed. The parameters range, which ensures the system stability, can be obtained. According to the pole distribution, the current and voltage control parameters that help to achieve the desired performance for the system can be acquired.

3.5 | Sensitivity assessment of the control parameters

The influence of the settling time ($t_{s.i}$, $t_{s.v}$) and damping factor (ζ_i, ζ_v), which are related to the PI controllers' parameters; on the roots' movement of the closed-loop models of the current control G_i^{BF} and the voltage control G_v^{BF} are investigated.

By the way, the characteristic equations of the current control closed-loop model can be expressed as follows:

$$\text{P controller}$$
$$1 + k_{p.i} G_T G_i = 0 \tag{25a}$$

$$\text{PI and feedforward controllers}$$
$$1 + C_i G_T G_i = 0 \tag{25b}$$

Also that of the voltage control closed-loop model is defined as follows:

$$1 + C_v G_i^{BF} G_v = 0 \tag{26}$$

The root plots of the current control characteristic equation are illustrated in Figure 6. In this figure, note that the black, red,

and blue curves represent the root locus of the PI and feedforward controllers-based CCL, which are obtained by fixing ζ_i at three different specified values and increasing $t_{s.i}$. But the green colour curve represents the root locus of the P-type CCL which is achieved by increasing $t_{s.i}$.

It can be observed from this figure that there is a complex couple that moves from the positive part of the real axis (unstable region) to the negative part (stable region) with a decrease in the imaginary part when $t_{s.i}$ increases. In addition, when increasing the damping coefficient ζ_i, the convergence in the imaginary part tends to disappear, thereupon a couple of the root is equal in value on the real axis of the negative portion, then they diverge with keeping negative real values. Furthermore, the third root of the PI-type and feedforward type CCL, with a real value, is increasing in the negative real part on the real axis.

In fact, the optimal controller's parameters can be chosen when a couple of the root is near the real-axis negative part, and the root angle has a small value, as illustrated in Figure 6. Hence, the value of the settling time $t_{s.i}$ can be selected according to the following condition:

$$t_{s.i} \ge 5.31 \times 10^{-4} s \tag{27}$$

Note that by comparison, the system stability range in the P-type-based CCL has a wide range of changes in the value of the response time, which allows for reaching the optimal response time while maintaining the system stability.

Figure 7 portrays the plots describing the influence of the settling time, $t_{s.v}$, and the damping factor, ζ_v, on the roots distribution of both types of voltage controllers, PI, and feedforward. These root-locus curves are obtained by fixing both $t_{s.i}$ and ζ_v at specified values, meanwhile, by increasing $t_{s.v}$. As seen, when the damping coefficient value ζ_v increases, as well as, the settling time $t_{s.i}$ is chosen in the section that achieves the CCL stability, the roots move to the stable region. Also, it can be noticed that the damping coefficient ζ_v can be selected to guarantee that the curve is in the part where all the roots are near the negative side of the real axis. Thus, the damping coefficient value can be determined as follows:

$$0.6 \le \zeta_v \tag{28}$$

As shown in Figure 7, that clarifies the possibility of determining the settling time $t_{s.v}$, which achieves VCL stability. It can be concluded that this parameter can be selected as

$$t_{s.v} \ge 3.078 \times 10^{-3} \text{ s} \tag{29}$$

In addition, the impact of the settling time $t_{s.v}$ and the damping factor ζ_v on the closed-loop model of the voltage control, G_v^{BF}, of both types of controllers, PI and feedforward considering bode plots are established, and the results are presented in Figure 8. Note that the curves representing the bode plots of the transfer function G_v^{BF} of both controllers' types shown in Figure 8a are obtained for specified fixed values of the settling time $t_{s.i}$ and the damping factor ζ_v while increasing the settling time $t_{s.v}$. But, Figure 8b depicts the bode plots of G_v^{BF} for both PI and feedforward controllers obtained by fixing $t_{s.v}$ and $t_{s.i}$ at specified values while increasing ζ_v.
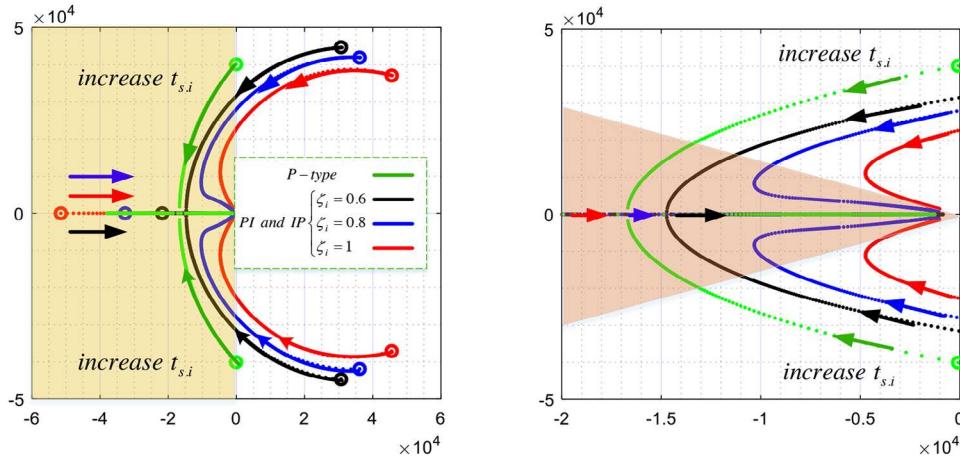
FIGURE 6 Poles' movements of the closed-loop transfer function of the current control with zoom-in.
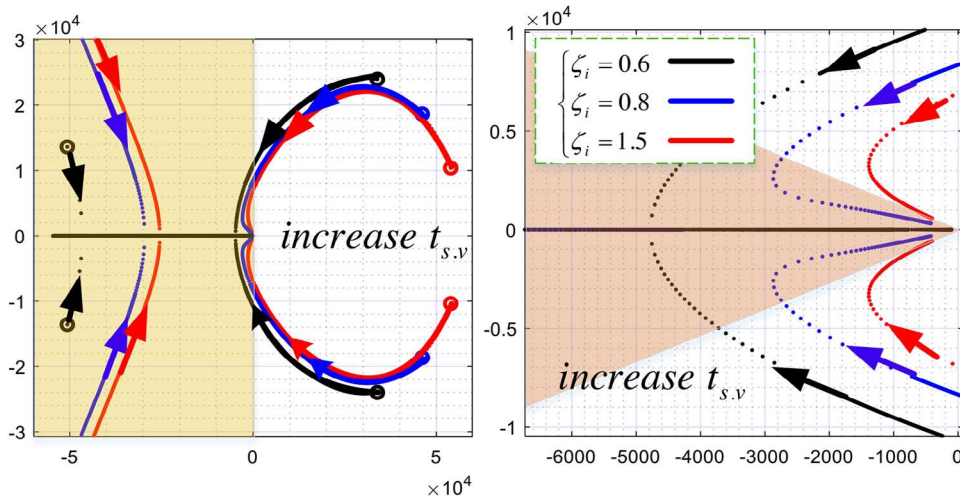

FIGURE 7 Poles' movements of the closed-loop transfer function of the voltage control with zoom-in.

As can be seen in Figure 8, a decrease in the response time while maintaining the damping value is proportional to an increase in the transfer function amplitude. The latter is considered to be in the resonant frequency domain with a decrease in the phase angle. Also, an increase in the damping value while maintaining the response time is proportional to an increase in the transfer function amplitude in the resonant frequency domain with an increase in the phase angle.

It is concluded by comparing the curves of both types of controllers that it is possible to reach the lowest response time that has a small amplitude in the resonant frequency domain and has a low angle value. Such performance is achieved by using the feedforward controller for the VCL.

3.6 | Robustness assessment of the designed controllers

The performance of the designed inner controller is investigated in terms of stability, considering variations in system parameters (i.e. L_1, r_1, C, and $t_{s,v}$). The results are shown in Figure 9.

Through this study, the range of the system parameters change can be determined, where the voltage control system remains stable. Obviously, the proposed design values of current and voltage controllers give high dynamic performance and robust stability under parameter variations.

3.7 | Control scheme discretization

It is well known that a controller should be discretized, at first, in order to be implemented in a microcontroller (MCU). Therefore, the discrete presentation of the current and voltage controllers is described below. By the way, the trapezoidal method is used to implement a discrete-time integrator, which can be presented by the following formulation:

$$y(k) = y(k-1) + \frac{T_s}{2}\left[u(k) + u(k-1)\right] \quad (30)$$

where $y(k)$ and $y(k-1)$ are the actual and previous output voltages, while $u(k)$ and $u(k-1)$ are the actual and previous input voltages of the integrator. k defines the operator of the
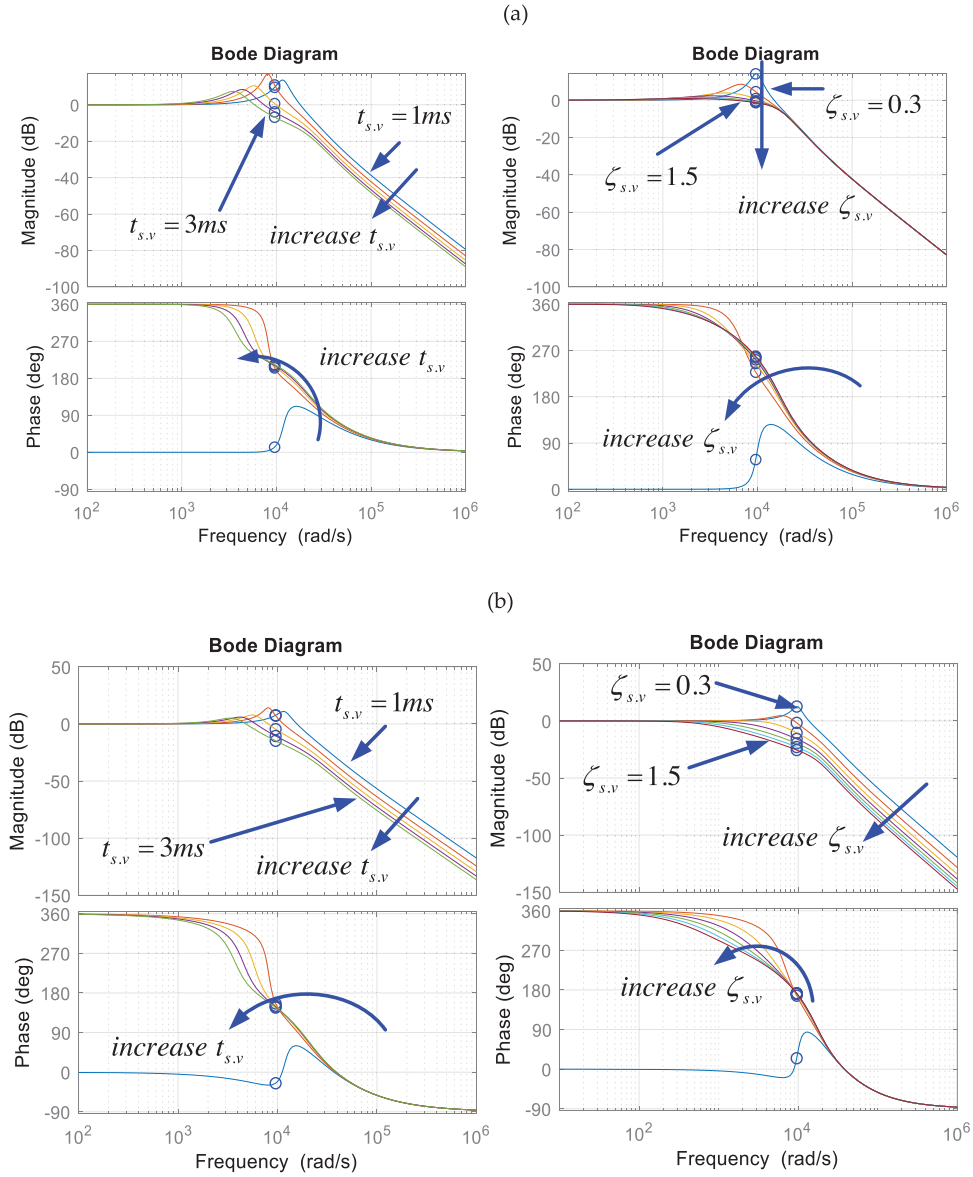
(a)

(b)

FIGURE 8 Bode plots of the voltage closed-loop model of (a) PI type and (b) feedforward controller type. PI, proportional-integral.

discrete-time domain. It is worth noting that in this method, the integral operator in the *s*-domain, that is, $1/s$, is approximated by [27]:

$$\frac{1}{s} = \frac{T_s}{2} \frac{1 + z^{-1}}{1 + z^{-1}} \tag{31}$$

where z denotes the discrete z-domain operator.

Accordingly, the model of the inner controller in discrete time can be presented by

$$\begin{cases} x(k) = x(k-1) + \left[v_c^{ref}(k) - v_c(k) \right] \\ i_{L1}^{ref}(k) = i_{L2}(k) - k_{p.v} v_c(k) + k_{i.v} \frac{T_s}{2} \left[x(k) + x(k-1) \right] \\ \bar{v}_{inv}^{ref}(k) = k_{p.i} \left[i_{L1}^{ref}(k) - i_{L1}(k) \right] + v_c(k) \\ D^{ref}(k) = \frac{\bar{v}_{inv}^{ref}(k)}{U_{DC}(k)} \end{cases} \tag{32}$$

where $x(k)$ is the state variable.

4 | SIMULATION RESULTS

For the purpose of evaluating the performance of the proposed inner controller for single-phase VSIs under different operating conditions, the system depicted in Figure 1 is built in MAT-LAB/Simulink. First, a comparative study between control with and without compensation is done for a resistive linear load of 100 Ω and non-linear load, and the results are illustrated in Figures 10–12. It is worth noting that the non-linear load is simulated with an uncontrolled rectifier feed an RC load of 100 Ω and 1000 μF.

Figures 10 and 11 show the capacitor voltage and the inductor current and their references in the presence of linear and non-linear loads, respectively, with and without compensation terms. One can see that the transient response with the compensation process is very fast with a zero steady-state error, and it suppresses the voltage overshoot and fluctuation while feeding a non-linear load. In addition, in Figure 12, which depicts
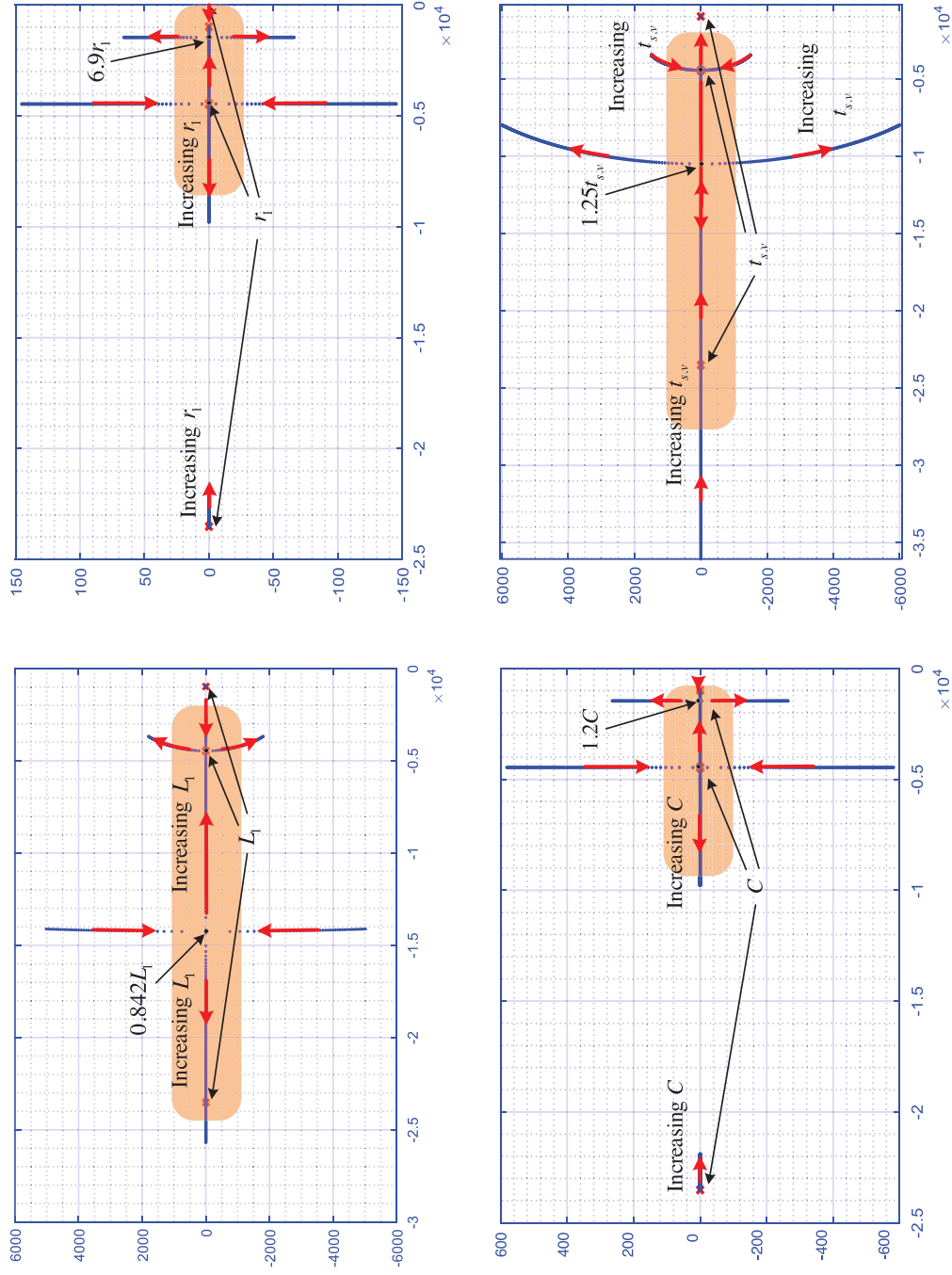
FIGURE 9 Root-locus corresponding to the change of the values of L_1, r_1, C, and $t_{s,v}$ parameters.
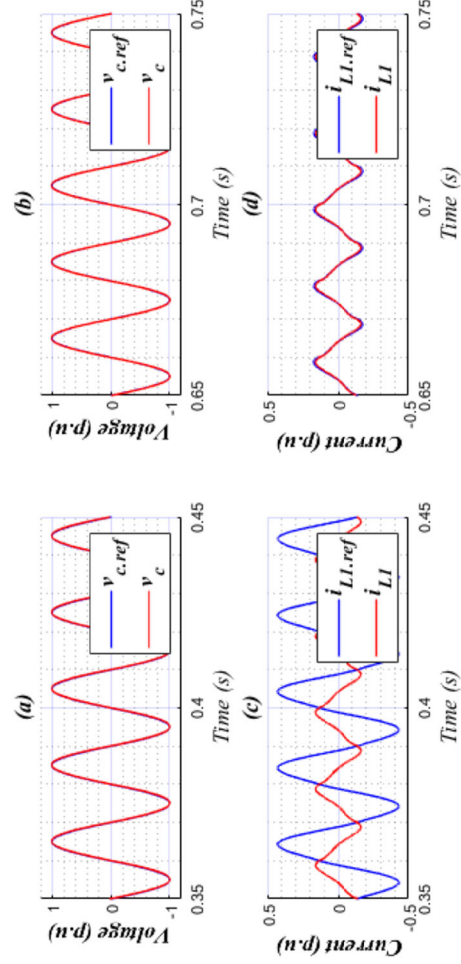

FIGURE 10 Results for the case of linear load: voltage (a) without compensation, (b) with compensation; and current (c) without compensation and (d) with compensation.
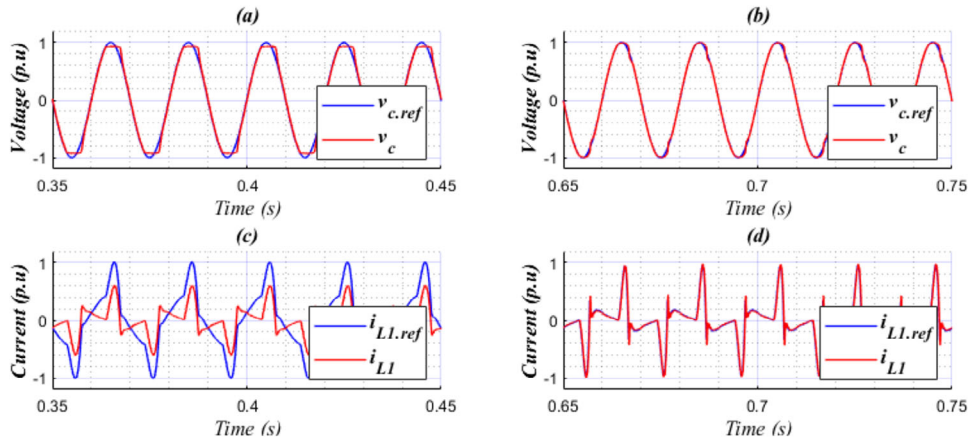
FIGURE 11 Results for the case of non-linear load: voltage (a) without compensation, (b) with compensation, and current (c) without compensation, (b) with compensation.
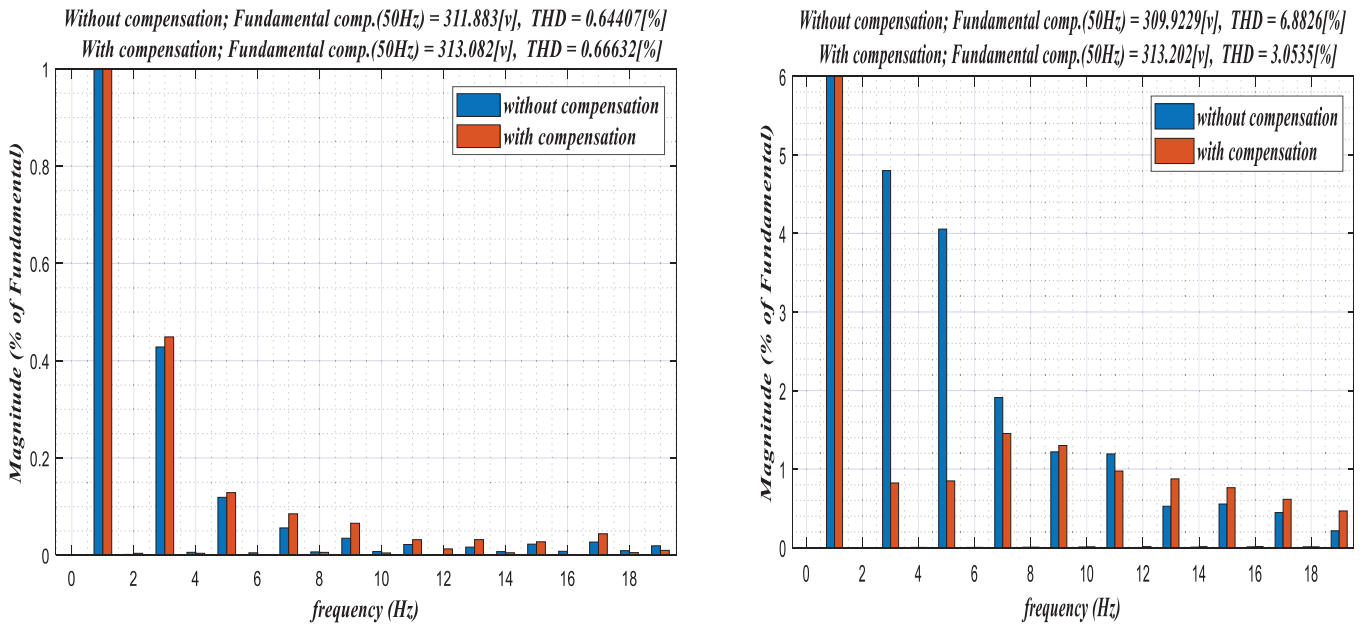

FIGURE 12 THD with and without compensation for the case of: (a) linear load, and (b) non-linear load. THD, total harmonic distortion.
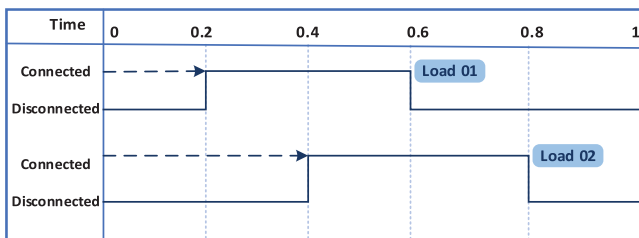

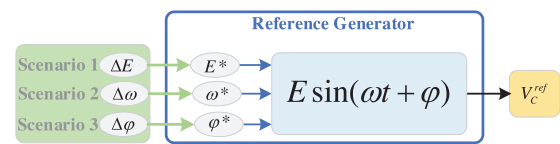**FIGURE 13** Performed scenarios of linear load connection and disconnection.

FIGURE 14 Performed scenarios of reference variations.

the voltage total harmonic distortion (THD), it can be seen that there is no big difference in the THD in both control with and without compensation in the case of linear load operation. But,

in the case of non-linear load, which is the main drawback of most existing research works, the THD decreases from 6.8826% to 3.0535% after introducing the compensation. Therefore, the THD value is below the limit (5%) defined by IEEE Standard 519 [28]. These outcomes confirm the necessity of introducing the compensation term for achieving accurate voltage and current tracking.
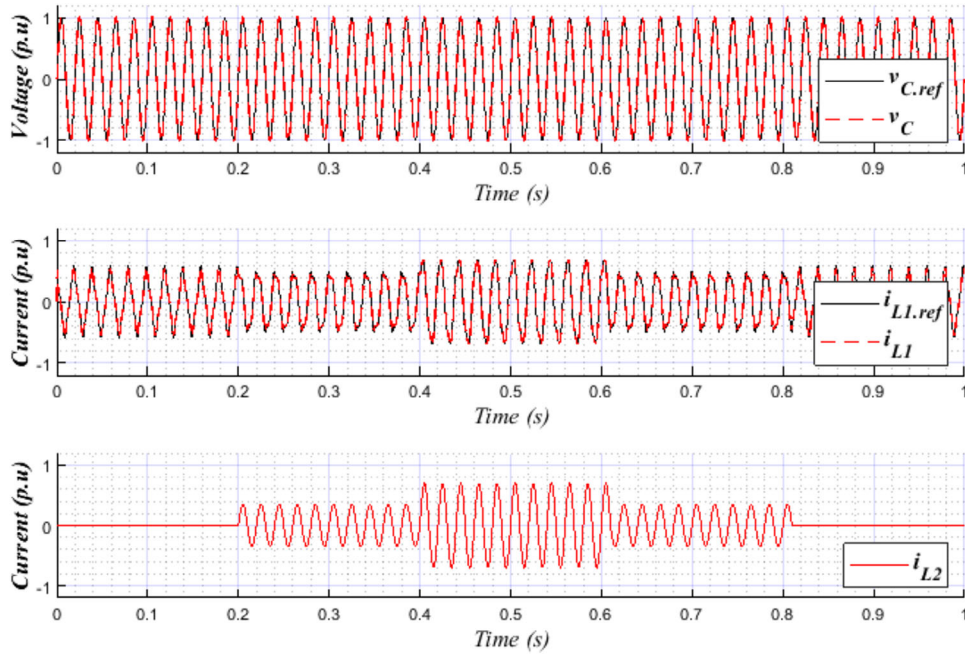
FIGURE 15   Simulation results in response to case 1.

TABLE 4   Parameters of the simulation study.

Parameters	Symbol	Unit	Value
Nominal voltage	E_n	V	220
Nominal frequency	f_n	Hz	50
Switching frequency	f_s	kHz	20
Simulation frequency	f_s	MHz	1
DC voltage	U_{DC}	V	495
Output filter capacitor	C	μF	23
Output filter inductor	L, r	mH, Ω	2, 1
Line impedance of DG	L	mH, Ω	0.5, 0.8
Voltage controller P gain	k_{pv}	–	0.1839
Voltage controller I gain	k_{pi}	–	183.87
Current controller P gain	k_{iv}	–	6.2831

Abbreviation: DG, distributed generator.

Since the previous results confirm the necessity of adopting the compensation term, the next simulations are conducted by introducing it into the designed control loops. The considered performance criteria for the designed control scheme are the transient and steady-state responses and the waveforms of the inverter's current and voltage. The implemented system parameters are summarized in Table 4. The following cases are considered for testing the designed controller:

- Case 01: Linear load change

Two linear loads of 500 W are supplied at different times as shown in Figure 13.

- Case 02: Non-linear load operation

Here, the VSI supplies a non-linear load represented by a diode-bridge rectifier with an RC load (100 Ω and 1000 μF) considered.

- Case 03: Voltage disturbances

Finally, the simulation is conducted in the presence of linear load, and different scenarios are carried on as demonstrated in Figure 14, where:

- Scenario 01: Voltage reference sag of 0.2 p. u (ΔE) of its fundamental amplitude ($E*$) is performed from 0.2 to 0.3 s.
- Scenario 02: A step change of the inverter frequency ($\Delta\omega$) from 50 to 100 Hz is set at $t = 0.5$ to 0.7 s.
- Scenario 03: A phase jump is introduced into the output voltage reference ($\Delta\varphi = \frac{\pi}{3}$) at $t = 0.9$ s.

The obtained simulation results show the controller-tracking performance regarding the instantaneous capacitor voltage and inductor currents, and their references in response to case studies, 1, 2, and 3, are portrayed in Figures 15–17, respectively. Figure 15 shows that an increase/decrease in power demand leads to an increase/decrease in the current, while the voltage is maintained stable. The controller follows the reference current established by the VCL even under feeding non-linear load as shown in Figure 16. But Figure 17a proves the effective and stable operation of the CCL, in which the inductor current tracks its reference current established by the VCL either if the amplitude/frequency values of the voltage reference varied or a phase jump happened. The same performance for the output voltage
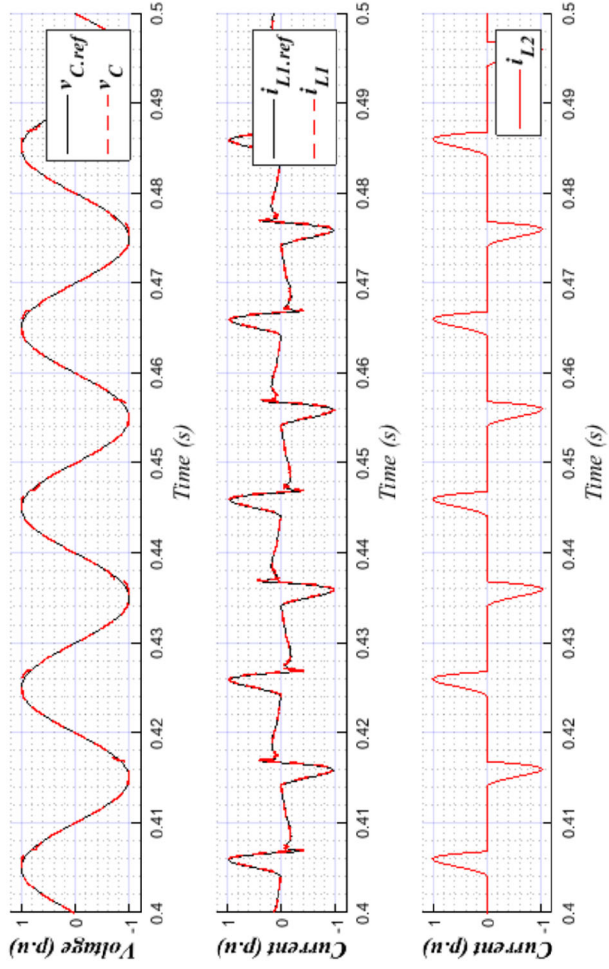
AÏT HAMMOUDA ET AL.

FIGURE 16 Simulation results in response to case 2.
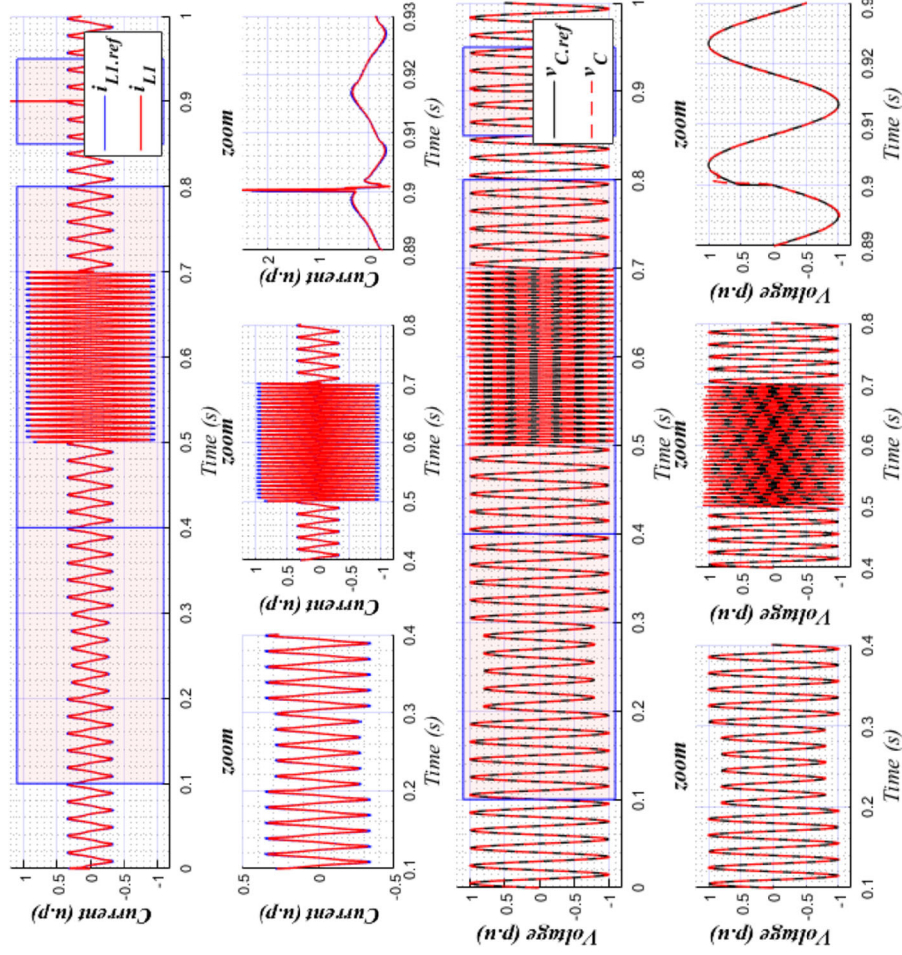

FIGURE 17 Simulation results in response to case 3 with the three scenarios.
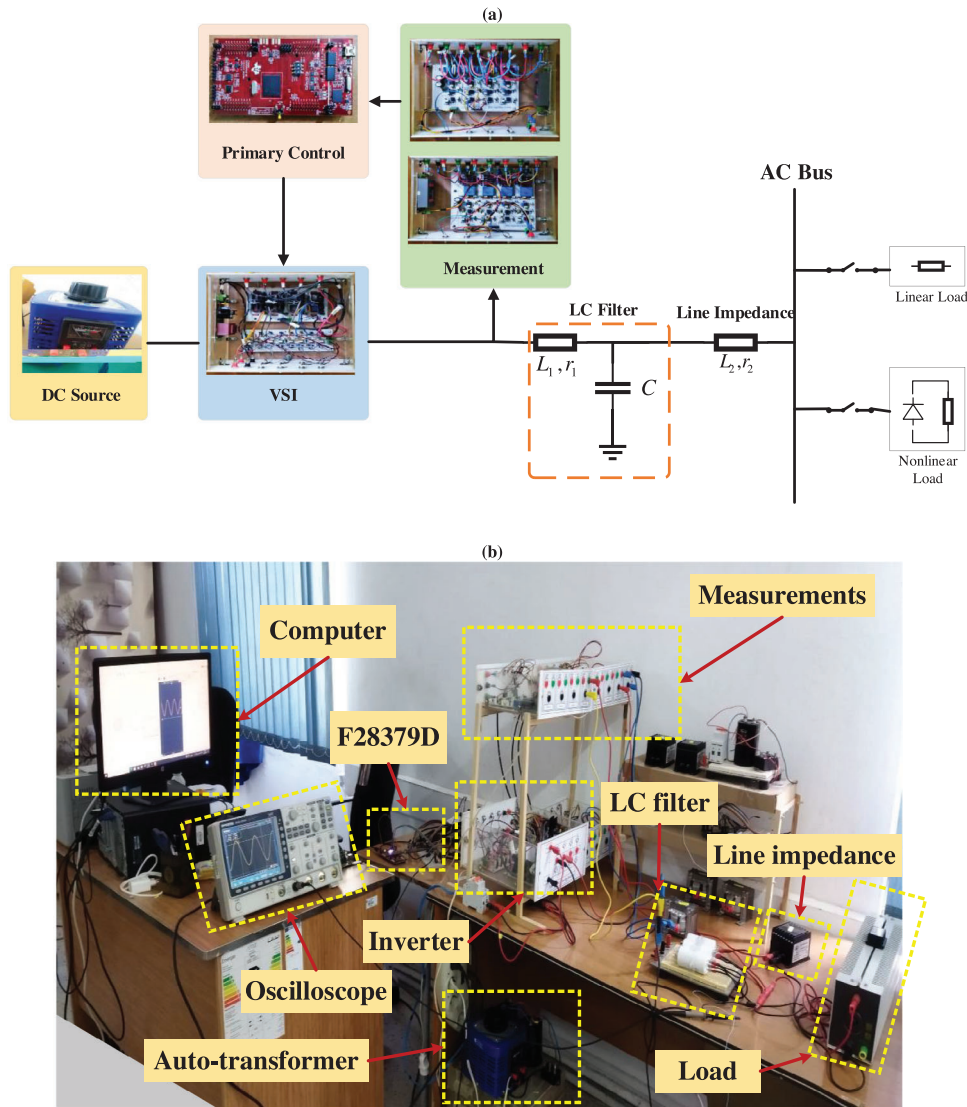
FIGURE 18   Experimental (a) real setup and (b) schematic setup.

and its reference is achieved as can be seen in Figure 17b. All the investigated cases demonstrate that the transient response of both voltage and current are well damped, lasting less than 2 ms (fast response) and without overshoot. Furthermore, the signals are relatively free of both, switching frequency and low-order harmonic distortion.

5 | EXPERIMENTAL RESULTS

To validate the effectiveness of the designed inner control scheme for controlling a single-phase VSI, an experimental setup of an islanded MG is conducted, as shown in Figure 18. As seen in Figure 18a, a VSI with LC filter fed by a DC source is associated with the AC bus via a line impedance, where the loads are linked. The designed inner control scheme, which consists of CCL with a P-type controller and a PI feedforward-type for the VCL, is implemented in a TMS320F2837xD MCU

family (LAUNCHXL-F28379D) with a switching frequency of 20 kHz. The system measurements are captured using voltage and current sensors and sent to the MCU through conditioning cards. The results are memorized in a memory card and plotted using MATLAB software. In Figure 18b, the different components included in the experimental setup are presented. Similar tests as the simulation study with the same parameters are considered.

Figures 19–21 show the obtained results of the proposed controller under the performed tests. The voltage performance shown in Figure 19 illustrates the precise tracking of the voltage reference when the load changes for both control strategies, with and without compensation. From the current waveforms, it can be noticed that the control strategy with compensation provides better performance than the control without compensation in terms of power quality and tracking; the actual current is almost matched with its reference. From Figure 20, one can notice that the control strategy with compensation
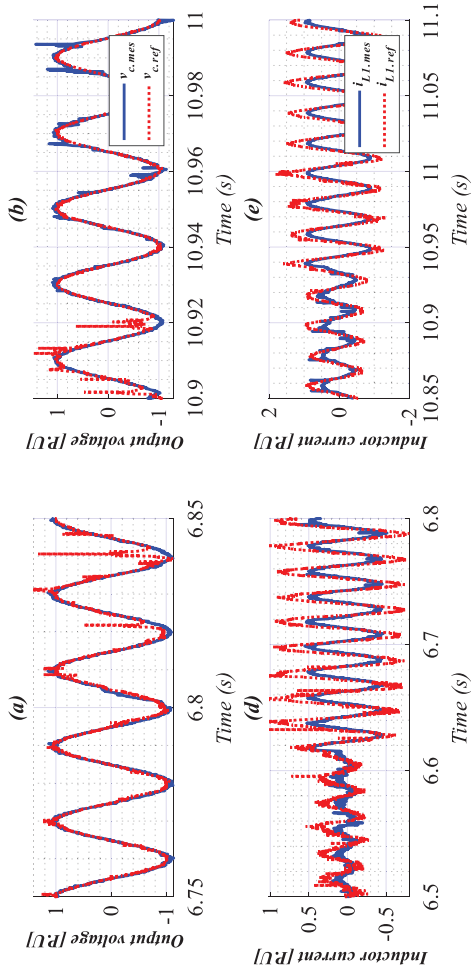
FIGURE 19 Experimental results for a linear load change; left without compensation, and right with compensation.
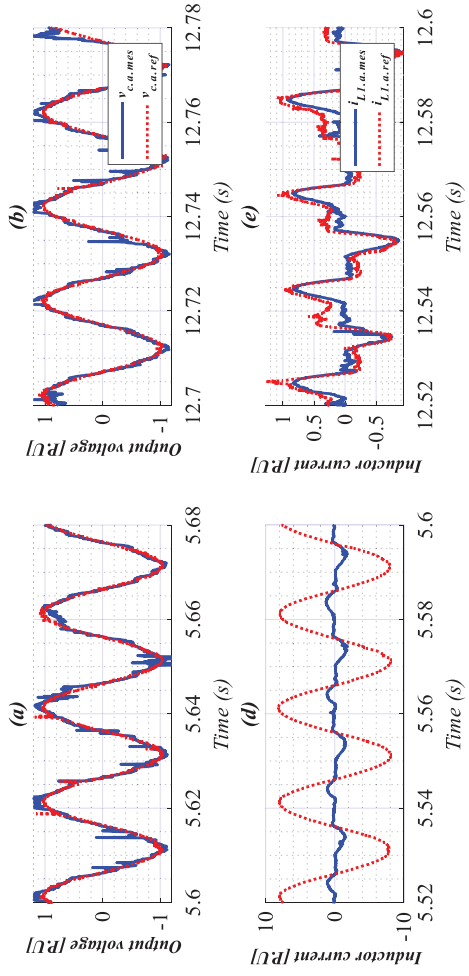

FIGURE 20 Experimental results for the case of non-linear load operation; left without compensation, and right without compensation.
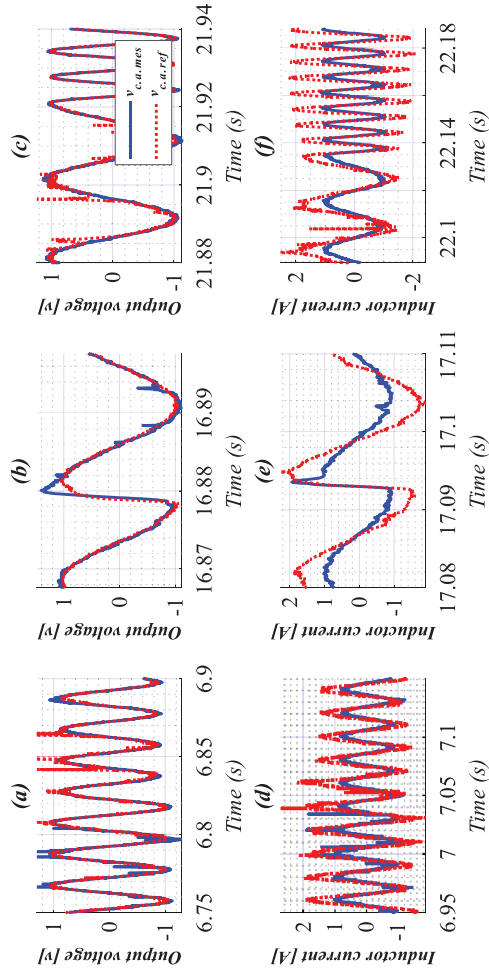

FIGURE 21 Experimental results for amplitude and frequency variations and phase jump.

ensures precise tracking of both output voltage and current references under non-linear load operation. But the controller without compensation performs good tracking of the output voltage reference, but poorly in current tracking.

Figure 21 validates the effective tracking of the output voltage and current for the control strategy with compensation under amplitude and frequency variations and phase jump. It can be seen that the voltage and current follow properly their references with good transient response against the stated disturbances. In addition, it can be observed that proper single-phase sinusoidal waveforms of the output voltage and current are achieved.

6 | CONCLUSION

An in-depth investigation of the modelling and design of voltage and CCLs considering three different types of PI controllers applied for a voltage-controlled single-phase VSI in MG was developed in this paper. The mathematical modelling of the CCL and VCL was provided. Therefore, the closed-loop models of the inner current control considering P, PI, and feedforward types, and the voltage control based on PI and feedforward controller types were derived. Besides, a detailed control design guideline of the CCL and VCL considering different PI controller types was proposed. Further, an analysis was presented, which enabled us to choose the P controller type for the CCL and the PI feedforward type for the VCL. The paper also investigated the impact of the compensation process, which has given a better insight into the output voltage and current, where the THD has decreased from 6.8826% to 3.0535% after introducing the compensation term. Simulations have been conducted using MATLAB/SimPowerSystem environment, to verify the effectiveness of the adopted controller. Also, experimental tests have been carried out to confirm the performance of the control purpose. The obtained simulation and experimental results, for both linear and non-linear loads, verify the analysis presented in this paper and have validated the effectiveness of the adopted control scheme. This proposed scheme has shown the following advantages; ease of implementation, a high tracking performance with good transient and steady-state responses, and robustness under different disturbances.

AUTHOR CONTRIBUTIONS
Camelia Ait Hammouda: Conceptualization; formal analysis; investigation; methodology; software; validation; writing—original draft; writing—review & editing. **Rafik Bradai**: Conceptualization; methodology; supervision; writing—original draft; writing—review & editing. **Ahmed Bendib**: Conceptualization; formal analysis; investigation; methodology; software; validation; visualization; writing—original draft; writing—review & editing. **Abdelhammid Kherbachi**: Conceptualization; methodology; writing—original draft; writing—review & editing. **Kamel Kara**: Conceptualization; supervision; writing—original draft; writing—review & editing. **Rachid Boukenoui**: Conceptualization; supervision; writing—original draft; writing—review & editing. **Hafiz Ahmed**: Project administration; methodology; writing—original draft; writing—review & editing.

ORCID
Abdelhammid Kherbachi https://orcid.org/0000-0002-6166-7744
Hafiz Ahmed https://orcid.org/0000-0001-8952-4190

REFERENCES
1. Castilla, M., García de Vicuña, L., Miret, J.: Microgrids design and implementation. In: Control of Power Converters in AC Microgrids. 1st ed., pp. 139–170, Ch5. Springer International Publishing (2019)
2. Moriarty, P., Honnery, D.: Renewable energy and energy reductions or solar geoengineering for climate change mitigation. Energies 15, 7315–7321 (2022)
3. Guerrero, J.M., De Vicuna, L.G., Matas, J., Castilla, M., Miret, J.: Output impedance design of parallel-connected UPS inverters with wireless load-sharing control. IEEE Trans. Ind. Electron. 52, 1126–1135 (2005)
4. He, J., Li, Y.W., Guerrero, J.M., Blaabjerg, F., Vasquez, J.C.: An islanding microgrid power-sharing approach using enhanced virtual impedance control scheme. IEEE Trans. Power Electron. 28, 5272–5282 (2013)
5. Bidram, A., Davoudi, A.: Hierarchical structure of microgirds control system. IEEE Trans. Smart Grid 3(4), 1963–1976 (2012). https://doi.org/10.1109/TSG.2012.2197425
6. Guerrero, J.M., Vasquez, J.C., Matas, J., Vicuna, L.G., Castilla, M.: Hierarchical control of droop-controlled AC and DC microgrids-A general approach toward standardization. IEEE Trans. Ind. Electron. 58(1), 158–172 (2011)
7. Guerrero, J.M., Chandorkar, M., Lee, T., Loh, P.C.: Advanced control architectures for intelligent microgrids—part I: Decentralized and hierarchical control. IEEE Trans. Ind. Electron. 60(4), 1254–1262 (2013)
8. Nazeri, A.A., Zacharias, P., Ibanez, F.M., Idrisov, I.: Paralleled modified droop-based voltage control source inverter for 100% inverter-based microgrids. In: 2021 IEEE Industry Application Society Annual Meeting (IAS), Vancouver, BC, Canada, pp. 1–8 (2021). https://doi.org/10.1109/IAS48185.2021.9677128
9. Ko, S.-H., Lee, S.R., Dehbonei, H., Nayar, C.V.: Application of voltage- and current-controlled voltage source inverters for distributed generation systems. IEEE Trans. Energy Convers. 21(3), 782–792 (2006). https://doi.org/10.1109/TEC.2006.877371
10. Chen, J., Yue, D., Dou, C., Chen, L., Weng, S., Li, Y.: A virtual complex impedance based P-V droop method for parallel-connected inverters in low-voltage AC microgrids. IEEE Trans. Ind. Inf. 17(3), 1763–1773 (2021). https://doi.org/10.1109/TII.2020.2997054
11. Ishaq, S., Khan, I., Rahman, S., Hussain, T., Iqbal, A., Elavarasan, R.M.: A review on recent developments in control and optimization of microgrids. Energy Rep. 8, 4085–4103 (2022)
12. Saxena, A., Chauhan, D.S.: Simulation and comparative analysis of single-phase H bridge micro inverters with conventional PI control and virtual output impedance control: A case study. Int. J. Power Electron. 14, 336–365 (2021)
13. Huber, L., Kumar, M., Jovanović, M.M.: Performance comparison of PI and P compensation in DSP-based average-current-controlled three-phase six-switch boost PFC rectifier. IEEE Trans. Power Electron. 30(12), 7123–7137 (2015). https://doi.org/10.1109/TPEL.2015.2389654
14. Guerrero, J.M., Lijun, H., Uceda, J.: Decentralized control for parallel operation of distributed generation inverters using resistive output impedance. IEEE Trans. Ind. Electron. 54, 994–1004 (2007)

15. Minetti, M., Rosini, A., Denegri, G.B., Bonfiglio, A., Procopio, R.: An advanced droop control strategy for reactive power assessment in islanded microgrids. IEEE Trans. Power Syst. 37(4), 3014–3025 (2022)

16. Li, X., Fang, J., Tang, Y., Wu, X., Geng, Y.: Capacitor-voltage feedforward with full delay compensation to improve weak grids adaptability of LCL-filtered grid-connected converters for distributed generation systems. IEEE Trans. Power Electron. 33(1), 749–764 (2018)

17. Batmani, Y., Khayat, Y., Najafi, S., Guerrero, J.M.: Optimal integrated inner controller design in AC microgrids. IEEE Trans. Power Electron. 37(9), 10372–10383 (2022)

18. Saim, A., Mellah, R., Houari, A., Machmoum, M., Djerioui, A.: Adaptive resonant based multi-loop control strategy for parallel distributed generation units in standalone microgrid application. Electr. Power Syst. Res. 143, 262–271 (2017)

19. Li, X., Lin, P., Tang, Y., Wang, K.: Stability design of single-loop voltage control with enhanced dynamic for voltage-source converters with a low LC-resonant-frequency. IEEE Trans. Power Electron. 33(11), 9937–9951 (2018). https://doi.org/10.1109/TPEL.2018.2794066

20. Hu, J., Shan, Y., Guerrero, J.M., Ioinovici, A., Chan, K.W., Rodriguez, J.: Model predictive control of microgrids – An overview. Renew. Sustain. Energy Rev. 136, 1–12 (2020)

21. Rajakumar, V., Anbukumar, K., Selwynraj, I.: Sliding mode controller-based voltage source inverter for power quality improvement in microgrid. IET Renew. Power Gener. 14(2), 1860–1872 (2020)

22. Akhavan, A., Golestan, S., Vasquez, J.C., Guerrero, J.M.: Passivity enhancement of voltage-controlled inverters in grid-connected microgrids considering negative aspects of control delay and grid impedance variations. IEEE J. Emerg. Sel. Topics Power Electron. 9(6), 6637–6649 (2021). https://doi.org/10.1109/JESTPE.2021.3065671

23. Liao, Y., Wang, X.: Evaluation of voltage regulators for dual-loop control of voltage-controlled VSCs. In: 2019 IEEE Energy Conversion Congress and Exposition (ECCE), Baltimore, MD, USA, pp. 5036–5042 (2019). https://doi.org/10.1109/ECCE.2019.8912561

24. Wang, X., Loh, P.C., Blaabjerg, F.: Stability analysis and controller synthesis for single-loop voltage-controlled VSIs. IEEE Trans. Power Electron. 32(9), 7394–7404 (2017)

25. Deng, H., Fang, J., Qi, Y., Tang, Y., Debusschere, V.: A generic voltage control for grid-forming converters with improved power loop dynamics. IEEE Trans. Ind. Electron. 70(4), 3933–3943 (2023). https://doi.org/10.1109/TIE.2022.3176308

26. Bendib, A., Kherbachi, A., Chouder, A., Ahmed, H., Kara, K.: Advanced control scheme and dynamic phasor modeling of grid-tied droop-controlled inverters. IET Renew. Power Gener. 1–19 (2022)

27. Chaparro, L.F., Akan, A.: Introduction to the design of discrete filters. In: Signals and Systems Using MATLAB-ch12. Elsevier (2019). https://doi.org/10.1016/B978-0-12-814204-2.00023-5

28. IEEE Std 519: Recommended practice and requirements for harmonic control in electric power systems (2003)